A Novel Modified Cotton Fabric with Durable Anti-Fouling Performance for Separation of Surfactant-stabilized Oil-in-water Emulsions

Pu Yang
Southwest University
Ruimin Hu
Southwest University
Yu Bin
Southwest University
Yiwei Sun
Southwest University
Yiping Liu
Southwest University
Ming Lu (lumingswu@126.com)
Southwest University https://orcid.org/0000-0002-9360-473X

Research Article

Keywords: Cotton fabric, protective layer, water permeability, emulsion separation

Posted Date: October 29th, 2021

DOI: https://doi.org/10.21203/rs.3.rs-1023069/v1

Version of Record: A version of this preprint was published at Cellulose on March 7th, 2022. See the published version at https://doi.org/10.1007/s10570-022-04488-8.

Abstract

Membrane applications for the separation of surfactant-stabilized emulsions are often constrained by a deficiency in permeability and anti-fouling properties. Herein, special wetted cotton fabric with a protective layer (P-MH@CF) for durable anti-fouling performance was designed by a two-step method, which was related to interfacial ion migration technology and unilateral spraying treatment. In detail, the immobilization of magnesium hydroxide caused the formation of the rough micro/nano structure of the cotton fabric surface. The stearic acid acted as a protective layer, like a quilt, protecting the membrane from contamination. Permeability of water and separation performance of P-MH@CF membrane were investigated systematically. For emulsion stabilized by SDS (SDS/Oil/H2O), the separation flux driven by gravity was approximately 500 L m -2 h -1 , and all separation efficiencies were over 99.3 %. CTAB/Oil/H2O emulsion and the Tween-60/Oil/H2O emulsion also could be successfully separated with high separation efficiency and separation flux. During the whole separation process, the oil droplets surrounded by surfactants were difficult to demulsify and gathered physically on the surface of the fabric to form a "creamy layer", which could be cleaned off so that the P-MH@CF membrane was not contaminated. In addition, the P-MH@CF membrane exhibited robust reusability for separation, which was promising for the remediation of oily wastewater containing surfactants.

Introduction

In recent years, a large volume of industrial oily wastewater containing surfactants has been produced in many fields, such as detergent, medicine, food, cosmetic, textile industries, while the reactors, storage tanks, and pipes have to be cleaned repeatedly (Ostertag et al. 2012; McClements and Jafari 2018). Oily wastewater has been a serious threat to the survival of aquatic animals and plants and human health. The solution to wastewater pollution has attracted the attention of researchers. As conventional oil/water separation technologies, flotation(Xiao et al. 2016), centrifugation(Pintor et al. 2014) and adsorption (Liu et al. 2015)suffer from the limitations owing to their poor selectivity for water phase and oil phase, low separation efficiency, and secondary pollution, respectively (Liu et al. 2019).

Membrane technology is considered one of the most promising technologies for treating oily wastewater, attributed to its satisfactory advantages such as excellent selectivity, small footprint, and cost-effectiveness (Cheng et al. 2020). Membrane materials prepared from cotton fabric as substrate is of great interest. Cotton fabrics consisting of cellulose are low-cost, abundantly sourced, flexible, environmentally friendly, and biodegradable. In addition, cotton fabrics with their inherent micropores assure initial membrane permeability. Hydrophilic cotton fabrics as one of the special wettability materials have been functionalized to not only achieve efficient separation of oil/water mixtures because the hydrating layer formed on the hydrophilic surface can prevent the contamination of hydrophobic pollutants (Pashley 1981; Wang et al. 2016), but also complete to separate surfactant-stabilized oil-in-water emulsions via the demulsification of the emulsions by ionic bonding formed by opposite charges between the membrane interface and surfactants. For emulsions with different types of surfactants, membranes with opposite electrical properties need to be designed to achieve the desired separation via

demulsification, which undoubtedly increases the production cost. Furthermore, electrostatic attraction could aggravate irretrievable contamination of the membrane and rapid reduction in separation efficiency. Wu et al. (Wu et al. 2018) grafted polydimethylaminoethyl methacrylate (pDMAEMA) to polypropylene film to obtain the PP-g-pDMAEMA film. When the SDS stabilized emulsion was separated, the flux recovery rate only reached about 60 % after one cycle. During separation of surfactant-stabilized emulsions, the hydrophilic tails of the surfactants tend to adhere to the hydrophilic membrane surface on account of the Coulombic force of attraction. The exposed hydrophobic head gradually reduces the polarity of the membrane surface and even makes the membrane hydrophobic, causing the separation membrane to be irreversibly contaminated. This deleterious membrane fouling cannot be simply washed away with water, resulting in a rapid decline in permeability and increased transmembrane pressure, and even membrane abandonment, thus limiting the development and application of such hydrophilic membrane materials (van der Marel et al. 2010; Liu et al. 2017). Therefore, how to prevent this deleterious fouling of the membrane surface without affecting its water permeability is an urgent problem.

There is an ancient Chinese poem about lotus: “Grow up from the filth but without being imbrued”. Inspired by the structure of natural lotus leaves, a rough surface is constructed and given asymmetric wettability to allow the transmission of water and the rejection of contamination. Herein, in this study micro-nano structured magnesium hydroxide was grown in situ on the fabric surface and a protective layer was constructed unilaterally, with the aim of improving the anti-fouling properties of the membrane. In detail, the growth and fixation of $Mg(OH)_2$ by interfacial ion migration technology modified the surface microstructure of cotton fabrics. Using stearic acid as a coating created the unilateral surface free energy at a lower threshold. The stearic acid layer acted as a protective barrier, like a quilt, covering the magnesium hydroxide. The polarity of the emulsion droplets of surfactant-stabilized oil-in-water was high and therefore oil droplets were not attracted to the membrane. The continuous aqueous phase successfully penetrated the membrane and the dispersed droplets gradually accumulated on the membrane surface. The droplets accumulated on top of the membrane due to gravity, which was a physical process. The “cream layer” that could be eliminated by physical flushing was reversible. P-MH@CF exhibited not only water permeability, stability and separation properties, but also excellent antifouling and recycling properties. The obtained membranes were investigated for their applicability for separation of emulsion stabilized by anionic, cationic, or nonionic surfactant separation.

Experimental

2.1. Materials

Plain woven cotton fabrics (CFs) (110 g m^{-2}, 52 warps per cm and 28 wefts per cm) were obtained from the market of China and desized in the 10 g/L sodium hydroxide (NaOH) solution at 100 ^{o}C for 60 min. NaOH, urea, stearic acid, reactive turquoise blue, sodium dodecyl sulfate (SDS), cetyltrimethy lammonium bromide (CTAB), and Tween-60 were purchased from China National Medicines Corporation Ltd. All chemicals and reagents were analytical grade had not been further purified.

2.2. Growth and immobilization of $Mg(OH)_2$

The cotton fabric (15 cm × 15 cm) was dipped in the 100 mL 7 % NaOH/12 % urea aqueous solution under the condition of -12 ^{o}C for 2 h. The treated fabrics were squeezed by the padding mangle (MU3C5T, China) and immediately immersed in a 40 wt % $MgCl_2 \bullet 6H_2O$ aqueous solution for 10 s. Then samples were transferred into the steam machine at 120 ^{o}C for 10 min. The obtained samples were washed with distilled water repeatedly, followed by drying at 40^{o}C.

2.3. Construction of unilateral protective layer

0.3 g of stearic acid was added to 100 mL ethanol solution with stirring for 5 min. The mixed solution was applied through spray-coating onto one side of the cotton fabrics with a spray bottle until the surface was covered evenly. A hydrophobic behavior was achieved after drying at 90 ^{o}C for 10 min. The above processes were repeated three times and the modified cotton fabric with a unilateral protective layer (P-MH@CF) was obtained.

2.4. Characterizations

The surface morphologies of samples were observed by scanning electron microscopy (SEM, Phenom Pro, Netherlands) with 10 kV accelerating voltage. The crystal structure of CFs was characterized by X-ray diffraction (XRD, TD-3500, China) with the monochromatized Cu·Kα_1 radiation (λ=0.154 nm) at 30 kV and 20 mA over the 2θ range of 5^{o}-70^{o} in steps of 0.02^{o}. The FTIR spectra were measured by Fourier transform infrared spectroscopy (Nicolet iS10, USA) with wavenumber range from 4000 cm^{-1} to 400 cm^{-1}. FTIR spectra of liquids were obtained by applying the sample to a KBr film and measuring it. Chemical states and compositions were analyzed by using X-ray photoelectron spectroscopy (XPS, Thermo Fisher Scientific, USA) equipped with an Al·Kα radiation source and a pass energy of 1253.6 eV under an ultra-high vacuum condition (10^{-9}-10^{-10} Torr). The static water contact angle was collected with a contact angle meter (OCA15EC, Germany) produced by Dataphysics Company in the condition that the volume of a deionized water droplet was about 3μL. Reliable sample angles were measured by averaging the measurements at five different locations on each sample surface.

2.5. Water permeability

According to the Young-Laplace equation (Eq. (1)), which P_L was calculated from, the mechanism of water droplet penetration could be more easily understood (Liu and Lange 2006; Zhou et al. 2013).

$$P_L = \frac{2\gamma \cos\theta}{r} \qquad (1)$$

where γ was the surface tension of the liquid, θ was the contact angle between the capillary wall and water drop, r represented the radius of the liquid.

2.6. Emulsions separation test

The as-prepared P-MH@CF was placed between the sand core funnel device (YAMAI, 250 mL, China) so that surfactant-stabilized oil-in-water emulsions were separated under gravity drive. Anionic surfactant (SDS), cationic surfactant (CTAB), and nonionic surfactant (Tween-60) were selected as emulsifiers. The separation performance of the membrane to emulsions stabilized by surfactants with different ionic types was evaluated in sequence. 1,2-dichloroethane (1.26 g cm^{-3}, weight oil), isooctane (0.69 g cm^{-3}, light oil) and xylene (0.86 g cm^{-3}, light oil) were selected as oil phase. Oil was dyed by Sudan III to differentiate it from water. Oil and water were mixed at a volume ratio of 1: 100. The mixture was treated by a high-speed homogenizer (XFK FSH-2A, China) at a speed of 13000 rpm. The gravity-driven separation efficiency and flux were calculated according to the following equation (2) and (3), respectively.

$$\text{Separation Efficiency} = \frac{V_P}{V_0} \times 100\% \qquad (2)$$

where V_0 was the initial volume of the water in the emulsion before separation and V_P was the volume of collected water after separation.

$$\text{Flux}(\text{L}/\text{m}^2\text{h}) = \frac{V}{St} \qquad (3)$$

where V (L) was the volume of filtrates, S (m^2, the effective filtration area was 11.9 cm^2) was the valid separation area of the membrane, t (h) was the separation time.

2.7. Protection performance test

To evaluate the performance of the protective layer of the membrane, the “cream layer” obtained after the separation of 50 mL, 100 mL, and 150 mL emulsion was observed by optical microscope respectively. The flux calculated after each 5 mL of the filtrate was collected to analyze the change of separation flux. The circulation test was performed by rinsing the “cream layer” on top of the membrane with deionized water and then separating the emulsion.

Results

3.1. Preparation of P-MH@CF membrane

The preparation mechanism of P-MH@CF, which combined interfacial ion migration technology and unilateral spraying treatment was illustrated in Scheme 1a. At -12 ^{o}C, the fabric (Scheme 1c-) was treated with 7 wt % NaOH/12 wt % urea solution for two hours. NaOH destroyed the intramolecular and intermolecular hydrogen bonds of cellulose, causing cellulose to swell and even partially dissolve (Scheme 1c-) (Cai and Zhang 2005; Fan et al. 2018). At the same time, hydroxide ions, sodium ions, and

alkali cellulose macromolecules constituted the internal ionic system of cotton fibers, also called an intra-membrane system (Scheme 1c-Ⅱ). Alkali cellulose macromolecules were immobilized within the membrane, while hydroxide ions and sodium ions were free to pass through the membrane. Treated cotton fabrics carrying OH^- were immersed in $MgCl_2•6H_2O$ aqueous solution. The solution outside the fibers contained magnesium ions and chlorine ions were considered as an extra-membrane system. There was a concentration gradient of mobile ions between inside and outside the membrane. Therefore, Mg^{2+} tended to migrate to the intra-membrane system and OH^- was inclined to move to the extra-membrane system. Mg^{2+} reacted with the OH^- immediately to form magnesium hydroxide at the interface of the surface of cotton fibers. As shown in SEM images, the raw CF surface was smooth, whereas the fibers of P-MH@CF were fully clad by $Mg(OH)_2$ with a micro-nano structure. Next, stearic acid was used as a finishing agent to create a protective layer on the unilateral surface of the fabric. Stearic acid imparted a low unilateral surface free energy value to the substrate and conferred a protective layer acting like a quilt.

Fig. 1a shows the FTIR spectra obtained for raw CF and P-MH@CF. The spectra of raw cotton and P-MH@CF were confirmed to be generally consistent, verifying that the primary structure of the treated cotton fabric remained unchanged. Characteristic peaks at 2968 cm^{-1} and 2918 cm^{-1} were belonging to the asymmetrical stretching vibration of the C-H bond in the $-CH_3$ and $-CH_2$ groups, respectively. The characteristic peak at 2848cm^{-1} was due to the symmetrical stretching vibration of the C-H bond in the $-CH_2$ group. The weak peaks at 1540cm^{-1} and 1457cm^{-1} were caused by the functional group of the carbonyl group (C=O) (Wen et al. 2018; Khattab et al. 2020; sharif et al. 2020), demonstrating that the stearic acid covering the fabric was in minor amounts. In the XRD pattern (Fig. 1b), both samples show three peaks centered around 14.94 °, 16.69 °, and 22.79 °, which were in accordance with the typical (1 -1 0), (1 1 0), and (2 0 0) peaks of natural cellulose fibers (French 2014). It was clear that the characteristic peaks indicated $Mg(OH)_2$ phase (2θ=19.22 °, 38.30 °, 50.78 °, and 58.96 °), which were attributed to their corresponding indices (0 0 1), (1 0 1), (1 0 2), and (1 1 0), respectively. From the wide scan spectrum (Fig. 1c), both CF and P-MH@CF had two main peaks of C1s and O1s. P-MH@CF has core level peaks of Mg 2p, Mg 2s, and Mg 1s at 49.6 eV, 88.1 eV, and 1303.2 eV, while Mg (KLL) peak appeared at about 306.1 eV (Keikhaei and Ichimura 2019). As in Fig. 1d, the C 1s spectrum was divided into four parts. The peaks were concentrated at 284.7 eV, 286.2 eV, corresponding to C-C/C-H, C-O of cellulose, respectively. In addition, the peaks are concentrated at 287.8 eV and 289.8 eV, which correspond to C=O and COO- respectively (Fan et al. 2018), demonstrating that stearic acid was covered onto the surface of the fabric. As shown in Fig. 1e and 1f, Mg 2p peak at 49.6 eV and the O 1s peak at 530.9 eV in XPS spectra was related to $Mg(OH)_2$ (Ardizzone et al. 1997; Zhu et al. 2011). The deposition of $Mg(OH)_2$ on the surface of cotton fabrics was further confirmed by XPS.

3.2. Water permeability

After dripping water onto the obverse side of the P-MH@CF membrane, the change of contact angle was recorded (Fig. 2a). The obverse side had hydrophobic abilities with a high WCA of about 141.1 °. When

the water was dropped onto the obverse side, the water droplet could spontaneously penetrate P-MH@CF from the hydrophobic side to the hydrophilic side. It took about 15.4 s for the water droplet to penetrate the membrane completely. Fig. 2c provides a set of images that also confirmed the transfer behavior of water in the air/air system.

3.3. Evaluation of the emulsion separation performance

A series of experiments were carried out to evaluate the separation performance of the P-MH@CF membrane. Emulsions were stabilized by three different ionic types of surfactants (SDS, CTAB, or Tween-60) respectively. The anionic surfactant stabilized emulsion (1,2-dichloroethane/SDS/H_2O) separation was evaluated at first.

The emulsion was directly injected into a sand core funnel device, and the volume of the emulsion was fixed as 100 mL. The emulsion was separated rapidly with water almost entirely penetrating the membrane while the oil droplets surrounded by SDS were blocked at the upper beaker. Optical microscopic images (Fig. 3e) of the emulsion and filtrate indicated that both emulsions contained numerous oil droplets, while the filtrate did not. Furthermore, as shown in the digital photographs, all the filtrates were clear and transparent. To demonstrate the absence of SDS in the filtrate, the samples were characterized by FTIR (Fig. 3b). To further evaluate the separation performance of the membrane, the change in the composition of the liquid before and after separation was tested. Characteristic peaks at 2971.73 cm^{-1} and 2868.71 cm^{-1} were mainly dominated by the symmetric and asymmetric stretching bands of C-H at the hydrophilic end of the surfactant. Peaks at 1200.15 cm^{-1} resulted from asymmetric S-O stretching, whereas the peaks at 1004.29 cm^{-1} corresponded to symmetric S-O stretching (Gao and Chorover 2010; Ramimoghadam et al. 2012; Warsi et al. 2020). Compared with the emulsion, the peaks of SDS (2971.73 cm^{-1}, 2868.71 cm^{-1}) were not highlighted in the curve of the filtrate. FTIR pattern of the filtrate was similar to that of distilled water, which showed that the separation effect was satisfactory.

For emulsions derived from different kinds of oil (Fig. 3a), 1,2-dichloroethane/SDS/H_2O, isooctane/SDS/H_2O, xylene/SDS/H_2O, the separation flux was 532 L m^{-2} h^{-1}, 609 L m^{-2} h^{-1} and 426 L m^{-2} h^{-1}, respectively. After calculation, separation efficiencies were more than 99.3 % each time. For emulsions by surfactants with different ionic types, as shown in Fig. 3c and 3d, CTAB/Oil/H_2O emulsions and the Tween-60/Oil/H_2O emulsions could also be successfully separated with high separation efficiency, indicating that the P-MH@CF membrane could be used to separate oily wastewater containing unspecified surfactants.

3.4. Separation mechanism

The separation process based on the simulation was demonstrated in Fig. 4a to further showing the mechanism of the P-MH@CF separation performance. In the separation process, water droplets dropped onto the hydrophobic side should form a hump (i.e., P_L) on the opposite side of the membrane pores (Fig. 4a left). Because of the presence of hydrophilic capillary force, the hydrophilic layer underneath would

eliminate P_L once the “hump” contacted the hydrophilic layer (Hou et al. 2019; Chen et al. 2019). Therefore, water permeated the membrane as a continuous phase. After surfactants were added to the oil-water mixture, the surfactant coating structure of the oil droplet was gradually assembled. Oil droplets surrounded by hydrophobic tails of surfactant tended to form the core, while the hydrophilic heads were exposed outside in contact with the aqueous environment. Oil droplets surrounded by surfactants were difficult to aggregate due to their thermodynamic stability. The $Mg(OH)_2$ decorated CF with an increase in micro/nanostructure and a reduction in the contact area between oil droplets and membrane (Zhang et al. 2013). Unilateral modification with stearic acid further exposed a large number of carbon chains on the surface of micro/nanostructures, resulting in a reduction in surface energy. Therefore, the stearic acid layer acted as a protective barrier, like a quilt, covering the magnesium hydroxide (Fig. 4a right). The polarity of the hydration layer was high. It was difficult for the oil droplets stabilized by surfactants to demulsify. Oil droplets surrounded by surfactants as a dispersed phase were rejected by the membrane. As time progressed, oil droplets physically accumulated on top of the membrane due to gravity, and the “cream layer” was gradually formed. It could be seen from the optical microscopic image that the “cream layer” was composed of undemulsified emulsion droplets (Fig. 4b right), while there were no oil droplets in the filtrate (Fig. 4b left).

3.5. Protection performance

The “cream layer” gradually formed on the surface of the membrane as the oil droplets physically accumulated. To evaluate the performance of the protective layer of the membrane, the “cream layer” obtained after the separation of 50 mL, 100 mL, and 150 mL emulsion was observed by optical microscope respectively. From the optical microscope pictures (Fig. 5b), it could be seen that the accumulation of emulsion droplets became more and more obvious with the increase of emulsion content, which showed that the “cream layer” was composed of undemulsified emulsion droplets. Oil droplets accumulated gradually driven by gravity on the membrane surface to form a “cream layer”, which facilitated to improve the separation efficiency to a certain extent. However, the “cream layer” also gradually covered the surface pores and reduced the effective separation area of the membranes, resulting in a gradual reduction of separation flux. It was also demonstrated by the flux calculated after each 5 mL of filtrate collected (Fig. 5a). As the separation process went on, flux gradually decreased from 1403 m^{-2} h^{-1} to about 412 L m^{-2} h^{-1}. Impressively, after rinsing with distilled water, the “cream layer” was easily washed off and the membrane was not contaminated by oil droplets (Fig. 5c). The separation flux of multiple cycles also proved that the “cream layer” was formed only through physical accumulation. There was no obvious decrease in liquid flux and separation efficiency after 10 cycles, which indicated robust reusability (Fig. 5d).

Conclusion

In summary, to resolve the permeability and anti-fouling deficiencies that exist in the membrane separation process, P-MH@CF membranes comprising unilateral protective layer were designed by interfacial ion migration technology and unilateral spraying treatment, which involved surface roughness

structure increased by immobilization of $Mg(OH)_2$ and relatively low surface energy modified by stearic acid. The stearic acid layer acted as a protective barrier, like a quilt, covering the magnesium hydroxide. When surfactant-stabilized oil-in-water emulsions were separated, the P-MH@CF membranes presented permeability of water and rejection of oil droplets. The P-MH@CF membrane exhibited the permeate flux of emulsions in the sequence of isooctane/SDS/H_2O (609 L m^{-2} h^{-1}) > 1,2-dichloroethane/SDS/H_2O (532 L m^{-2} h^{-1}) > xylene/SDS/H_2O (426 L m^{-2} h^{-1}) with separation efficiency of 99.6 %, 99.5 % and 99.6 %, respectively. The P-MH@CF membranes were effective for separating oil-in-water emulsions stabilized by SDS, CTAB, or Tween-60, with a high separation flux and efficiency. Furthermore, the “cream layer” formed by the settling of oil droplets during the separation process could also be easily washed off and the membranes showed excellent stability and reusability. These results proved that P-MH@CF membranes were an expected separation material and showed a vast range of application prospects in the separation of oily wastewater containing unspecified surfactants.

Declarations

Acknowledgements

Pu Yang and Ruimin Hu contributed equally to this work. This work was financially supported by Government-Sponsored Visiting Scholar Research Program (201908505032, 202006995001).

Declaration of interests

The authors declare that they have no known competing financial interests or personal relationships that could have appeared to influence the work reported in this paper.

References

1. Ardizzone S, Bianchi CL, Fadoni M, Vercelli B (1997) Magnesium salts and oxide: an XPS overview. Appl Surf Sci 119:253–259. https://doi.org/10.1016/s0169-4332(97)00180-3
2. Cai J, Zhang L (2005) Rapid dissolution of cellulose in LiOH/urea and NaOH/urea aqueous solutions. Macromol Biosci 5:539–548. https://doi.org/10.1002/mabi.200400222
3. Chen C, Weng D, Mahmood A, et al (2019) Separation Mechanism and Construction of Surfaces with Special Wettability for Oil/Water Separation. ACS Appl Mater Interfaces 11:11006–11027. https://doi.org/10.1021/acsami.9b01293
4. Cheng X, Sun Z, Yang X, et al (2020) Construction of superhydrophilic hierarchical polyacrylonitrile nanofiber membranes by: In situ asymmetry engineering for unprecedently ultrafast oil-water emulsion separation. J Mater Chem A 8:16933–16942. https://doi.org/10.1039/d0ta03011b
5. Fan T, Qian Q, Hou Z, et al (2018) Preparation of smart and reversible wettability cellulose fabrics for oil/water separation using a facile and economical method. Carbohydr Polym 200:63–71. https://doi.org/10.1016/j.carbpol.2018.07.040

6. French AD (2014) Idealized powder diffraction patterns for cellulose polymorphs. Cellulose 21:885–896. https://doi.org/10.1007/s10570-013-0030-4
7. Gao X, Chorover J (2010) Adsorption of sodium dodecyl sulfate (SDS) at ZnSe and α-Fe2O3 surfaces: Combining infrared spectroscopy and batch uptake studies. J Colloid Interface Sci 348:167–176. https://doi.org/10.1016/j.jcis.2010.04.011
8. Hou L, Wang N, Man X, et al (2019) Interpenetrating janus membrane for high rectification ratio liquid unidirectional penetration. ACS Nano 13:4124–4132. https://doi.org/10.1021/acsnano.8b08753
9. Keikhaei M, Ichimura M (2019) Fabrication of Mg(OH) 2 thin films by electrochemical deposition with Cu catalyst. Thin Solid Films 681:41–46. https://doi.org/10.1016/j.tsf.2019.04.046
10. Khattab TA, Mohamed AL, Hassabo AG (2020) Development of durable superhydrophobic cotton fabrics coated with silicone/stearic acid using different cross-linkers. Mater Chem Phys 249:122981. https://doi.org/10.1016/j.matchemphys.2020.122981
11. Liu B, Lange FF (2006) Pressure induced transition between superhydrophobic states: Configuration diagrams and effect of surface feature size. J Colloid Interface Sci 298:899–909. https://doi.org/10.1016/j.jcis.2006.01.025
12. Liu L, Pan Y, Bhushan B, Zhao X (2019) Mechanochemical robust, magnetic-driven, superhydrophobic 3D porous materials for contaminated oil recovery. J Colloid Interface Sci 538:25–33. https://doi.org/10.1016/j.jcis.2018.11.066
13. Liu X, Ge L, Li W, et al (2015) Layered double hydroxide functionalized textile for effective oil/water separation and selective oil adsorption. ACS Appl Mater Interfaces 7:791–800. https://doi.org/10.1021/am507238y
14. Liu Y, Su Y, Cao J, et al (2017) Antifouling, high-flux oil/water separation carbon nanotube membranes by polymer-mediated surface charging and hydrophilization. J Memb Sci 542:254–263. https://doi.org/10.1016/j.memsci.2017.08.018
15. McClements DJ, Jafari SM (2018) Improving emulsion formation, stability and performance using mixed emulsifiers: A review. Adv Colloid Interface Sci 251:55–79. https://doi.org/10.1016/j.cis.2017.12.001
16. Ostertag F, Weiss J, McClements DJ (2012) Low-energy formation of edible nanoemulsions: Factors influencing droplet size produced by emulsion phase inversion. J Colloid Interface Sci 388:95–102. https://doi.org/10.1016/j.jcis.2012.07.089
17. Pashley RM (1981) Hydration forces between mica surfaces in aqueous electrolyte solutions. J Colloid Interface Sci 80:153–162. https://doi.org/10.1016/0021-9797(81)90171-5
18. Pintor AMA, Vilar VJP, Botelho CMS, Boaventura RAR (2014) Optimization of a primary gravity separation treatment for vegetable oil refinery wastewaters. Clean Technol Environ Policy 16:1725–1734. https://doi.org/10.1007/s10098-014-0754-3
19. Ramimoghadam D, Hussein MZ Bin, Taufiq-Yap YH (2012) The effect of sodium dodecyl sulfate (SDS) and cetyltrimethylammonium bromide (CTAB) on the properties of ZnO synthesized by hydrothermal method. Int J Mol Sci 13:13275–13293. https://doi.org/10.3390/ijms131013275

20. sharif R, Mohsin M, Ramzan N, et al (2020) Synthesis and Application of Fluorine-free Environment-friendly Stearic Acid-based Oil and Water Repellent for Cotton Fabric. J Nat Fibers 00:1–16. https://doi.org/10.1080/15440478.2020.1787918
21. van der Marel P, Zwijnenburg A, Kemperman A, et al (2010) Influence of membrane properties on fouling in submerged membrane bioreactors. J Memb Sci 348:66–74. https://doi.org/10.1016/j.memsci.2009.10.054
22. Wang Z, Jin J, Hou D, Lin S (2016) Tailoring surface charge and wetting property for robust oil-fouling mitigation in membrane distillation. J Memb Sci 516:113–122. https://doi.org/10.1016/j.memsci.2016.06.011
23. Warsi F, Islam MR, Alam MS, Ali M (2020) Exploring the effect of hydrophobic ionic liquid on aggregation, micropolarity and microviscosity properties of aqueous SDS solutions. J Mol Liq 310:113132. https://doi.org/10.1016/j.molliq.2020.113132
24. Wen R, Zhang W, Lv Z, et al (2018) A novel composite Phase change material of Stearic Acid/Carbonized sunflower straw for thermal energy storage. Mater Lett 215:42–45. https://doi.org/10.1016/j.matlet.2017.12.008
25. Wu J, Wei W, Li S, et al (2018) The effect of membrane surface charges on demulsification and fouling resistance during emulsion separation. J Memb Sci 563:126–133. https://doi.org/10.1016/j.memsci.2018.05.065
26. Xiao C, Si L, Liu Y, et al (2016) Ultrastable coaxial cable-like superhydrophobic mesh with self-adaption effect: Facile synthesis and oil/water separation application. J Mater Chem A 4:8080–8090. https://doi.org/10.1039/c6ta01621a
27. Zhang F, Zhang W Bin, Shi Z, et al (2013) Nanowire-haired inorganic membranes with superhydrophilicity and underwater ultralow adhesive superoleophobicity for high-efficiency oil/water separation. Adv Mater 25:4192–4198. https://doi.org/10.1002/adma.201301480
28. Zhou H, Wang H, Niu H, Lin T (2013) Superphobicity/philicity Janus Fabrics with Switchable, Spontaneous, Directional Transport Ability to Water and Oil Fluids. Sci Rep 3:2964. https://doi.org/10.1038/srep02964
29. Zhu Y, Wu G, Zhang YH, Zhao Q (2011) Growth and characterization of Mg(OH) 2 film on magnesium alloy AZ31. Appl Surf Sci 257:6129–6137. https://doi.org/10.1016/j.apsusc.2011.02.017

Figures

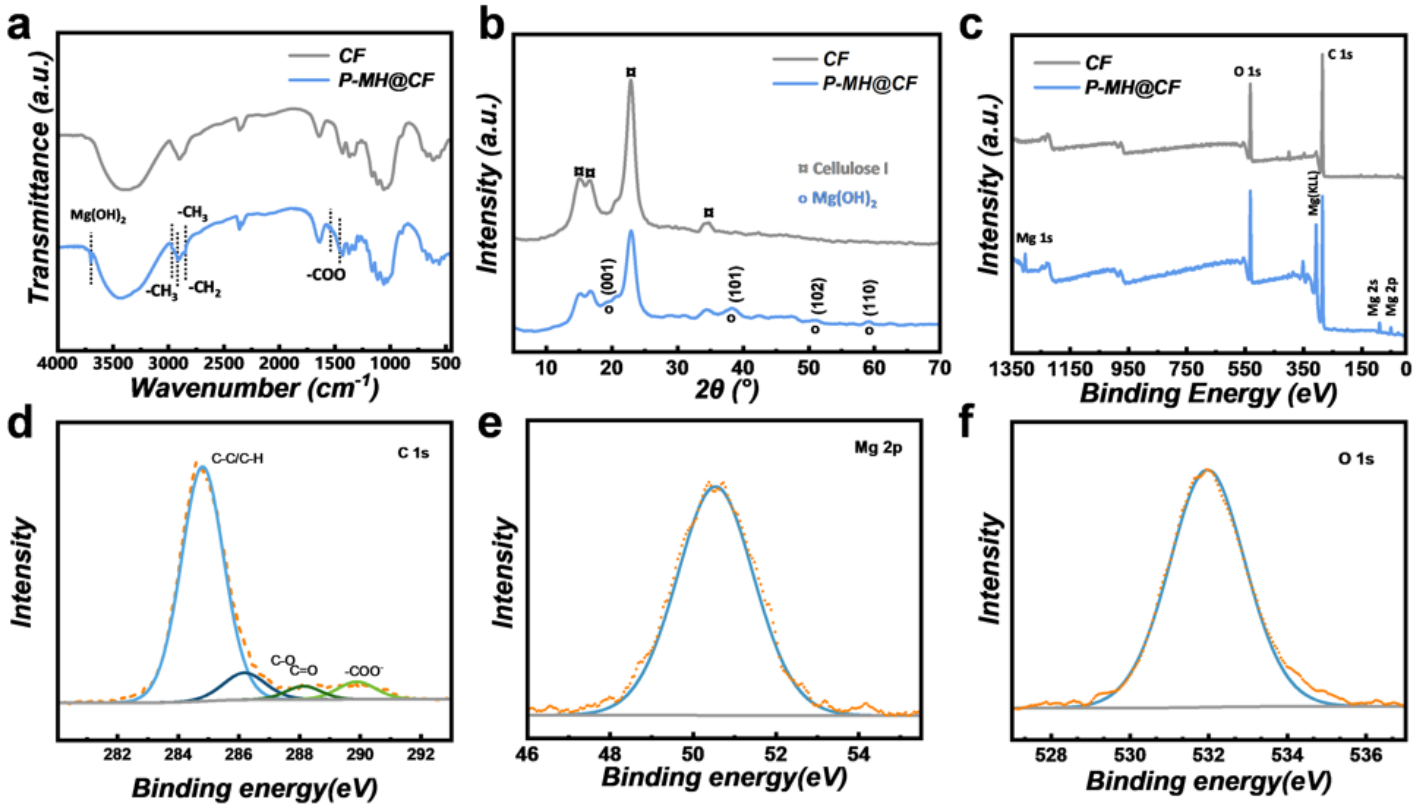

Figure 1

(a) FTIR (b)XRD (c) XPS survey spectra of raw CF and P-MH@CF membrane. (d) C 1s, (e) O 1s, and (f) Mg 2p of P-MH@CF membrane.

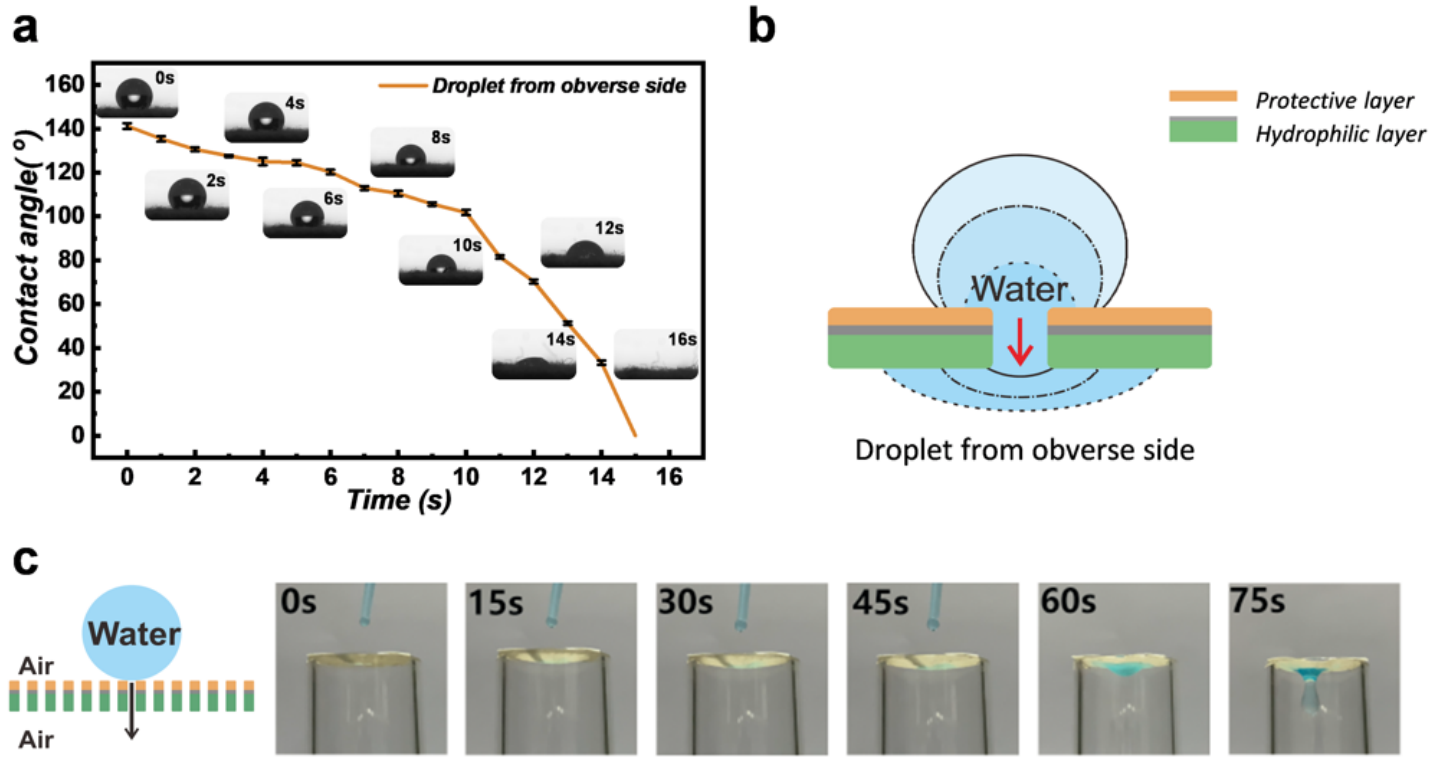

Figure 2

(a) Water contact angle changes during the dropping of water onto the obverse side of the P-MH@CF membrane. (b) Schematic diagram of the mechanism of the wetting process. (c) Photograph of the behavior of water on P-MH@CF membrane.

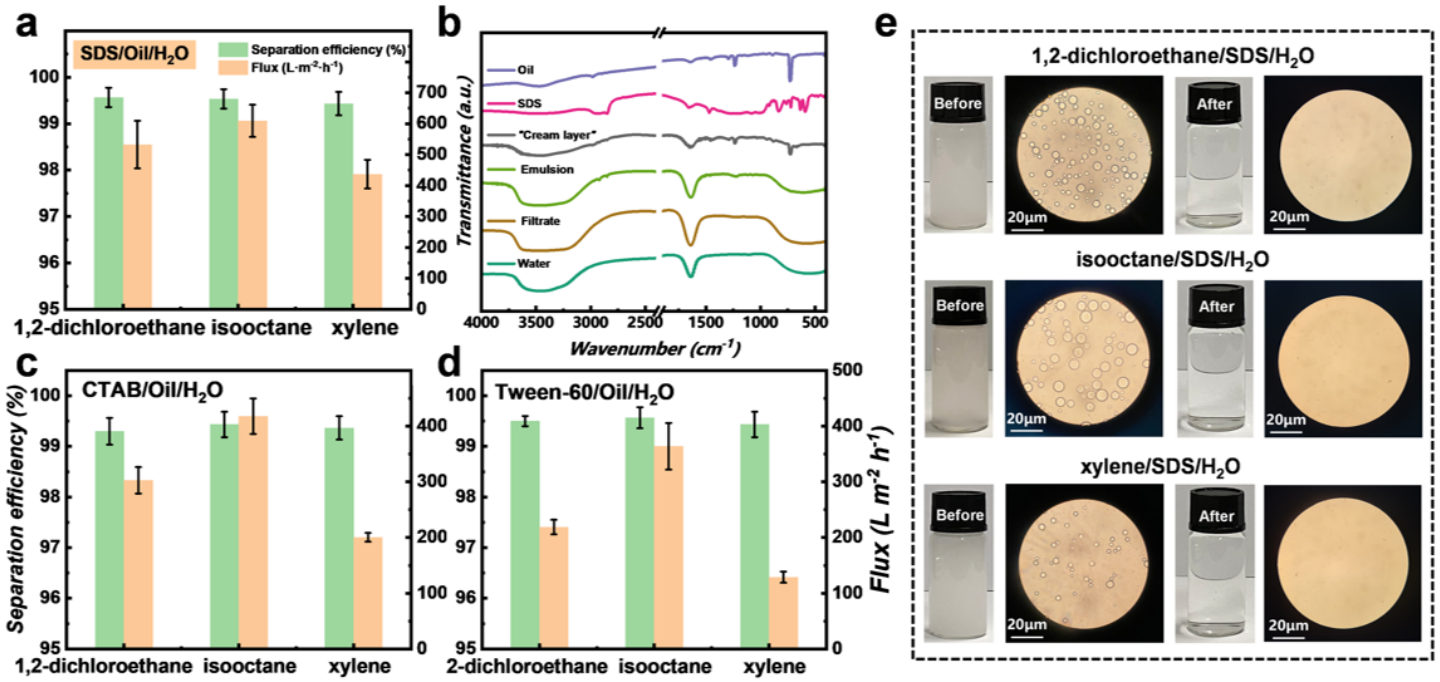

Figure 3

Separation efficiency and permeation flux for emulsions stabilized by (a) SDS, (c) CTAB, and (d) Tween-60, respectively, under the driving of gravity. (b) FTIR spectra of oil, SDS, “cream layer”, emulsion, filtrate, and water. (e) Photographs and optical microscopic images of the surfactant-stabilized emulsions before and after separation.

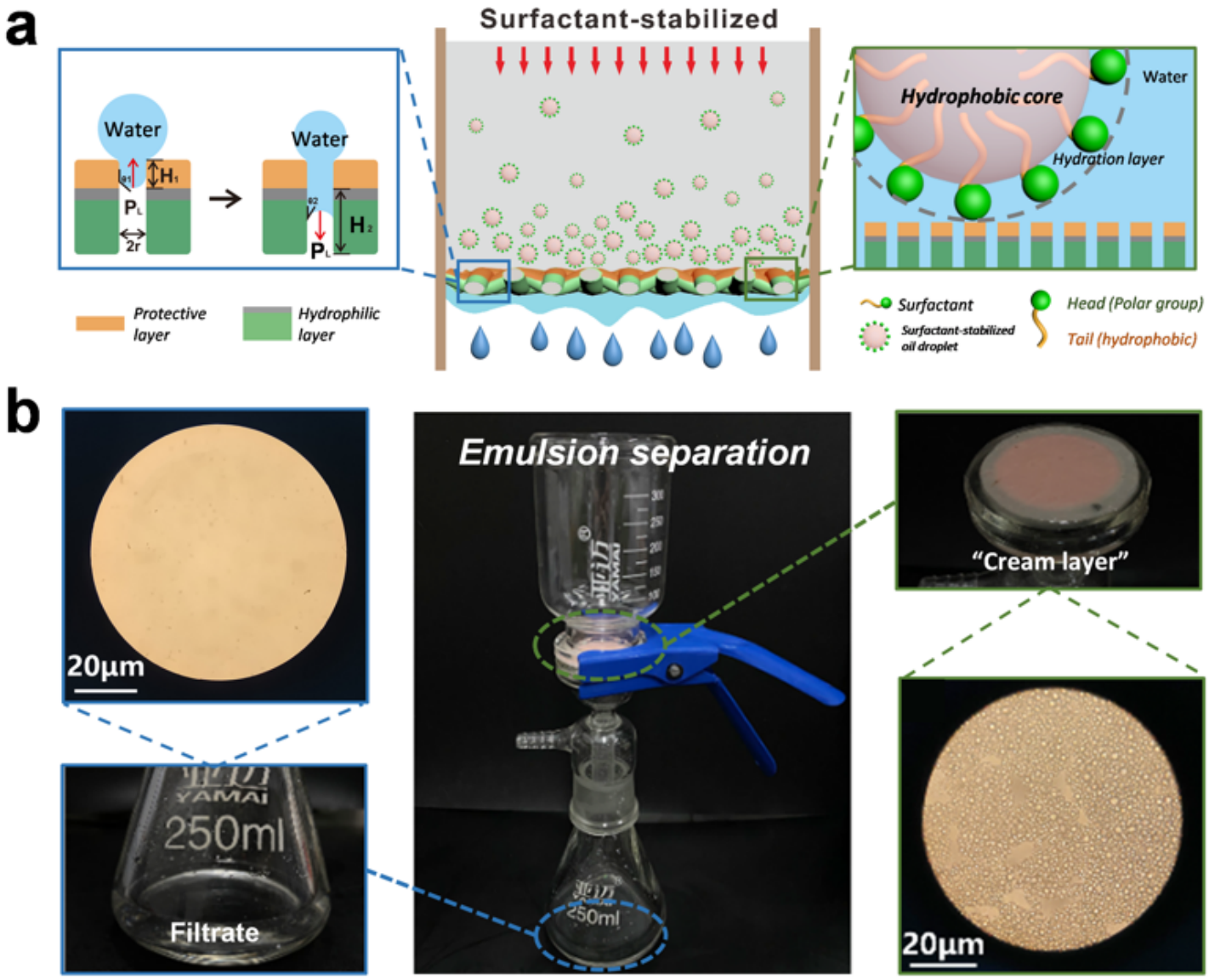

Figure 4

(a) Schematic diagram of the emulsions separation mechanism. (b) Photographs of the emulsion before and after separation and optical microscopic images of the filtrate and “cream layer” resulting from the separation.

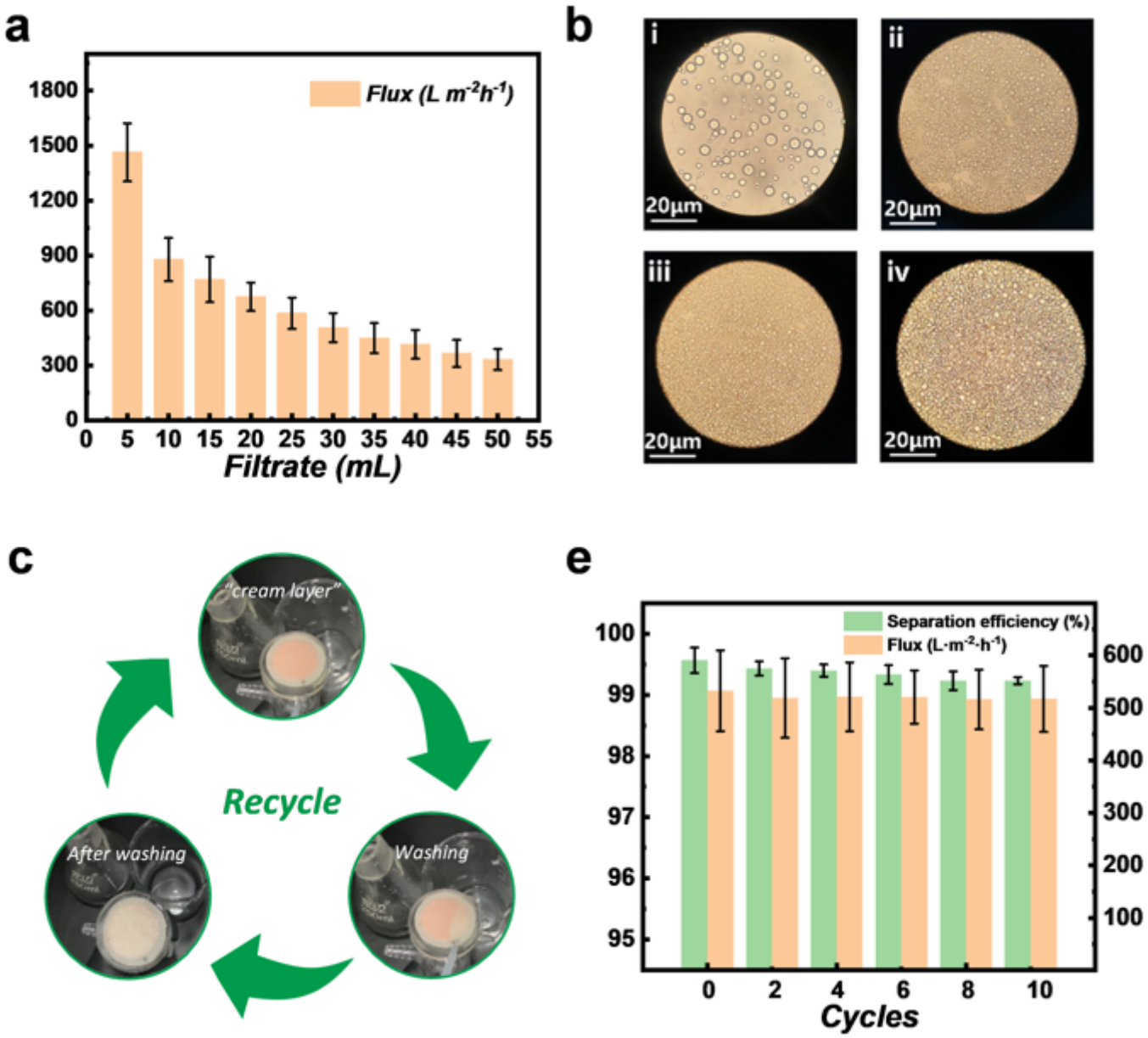

Figure 5

(a) Flux was calculated after every 5mL of filtrate collected during separation. (b) Optical microscopic images of the emulsion (b-□) and “cream layer” obtained after the separation of 50mL (b-□), 100mL (b-□), and 150mL (b-□) emulsion. (c) Photographs of the process of rinsing off the “cream layer” with water. (d) The recyclability of P-MH@CF membrane for surfactant-stabilized emulsions separation.

Supplementary Files

This is a list of supplementary files associated with this preprint. Click to download.

- Graphicalabstract.png
- sheme1.png